11th International Conference
1-3 July 2013
Pisa
RASD 2013

NONLINEAR STOCHASTIC DYNAMICAL POST-BUCKLING ANALYSIS OF UNCERTAIN CYLINDRICAL SHELLS

E. Capiez-Lernout[1*], C. Soize[1] and M.-P. Mignolet[2]

[1]Laboratoire Modélisation et Simulation Multi-Echelle, MSME UMR 8208 CNRS
Université Paris-Est
5 bd Descartes, 77454 Marne-la-Vallée Cedex 02, France
E-mail: evangeline.capiezlernout@univ-paris-est.fr, christian.soize@univ-paris-est.fr

[2]SEMTE, Faculties of Mechanical and Aerospace Engineering
Arizona State University,
Tempe, Arizona 85287-6106, USA
E-mail: marc.mignolet@asu.edu

Keywords: uncertainties, stochastic excitation, geometrical nonlinearities, dynamic post-buckling

ABSTRACT

This paper presents the nonlinear dynamical post-buckling analysis of an uncertain cylindrical shell. The proposed approach is adapted to the dynamical analysis of geometrically nonlinear structures subjected to a stochastic ground-based motion in the presence of both system parameter uncertainties and model uncertainties. The structure is modeled by a large finite element model using 3D elasticity theory. The ground-based motion is represented by a Gaussian centered non-stationary second-order stochastic process. Then, a reduced-order basis is constructed using the POD (Proper Orthogonal Decomposition) analysis of a nonlinear static reference response combined with selected linear eigenmodes of vibrations. The mean reduced-order nonlinear computational model is then explicitly constructed. A positive-definite operator involving the nonlinear stiffness of the structure is defined, allowing the nonparametric probabilistic approach to be used for constructing the uncertain nonlinear reduced-order computational model. The dispersion parameter controlling the level of stiffness uncertainty is a scalar which has been previously identified experimentally in a nonlinear static context. Finally, the instantaneous spectral density power of the dynamical response is analyzed in order to quantify the influence of both geometrical nonlinearities and random uncertainties on the stochastic dynamical response.

1. INTRODUCTION

The focus of this research is on the post-buckling dynamical behavior of thin cylindrical shells, which is currently a subject of interest, since a discrepancy between the experimental observations and the predicted observations can be observed, due to the particular sensitivity of thin cylindrical shell structures to the presence of initial imperfections. Note that for

cylindrical shells of very small thickness, the geometrically nonlinear effects induced by large strains and large displacements must be taken into account. Numerous sensitivity analyses to standard geometric imperfections can be found in the literature, distinguishing several classes of external loads such as axial compression [1–3], pressure load [4, 5] and shear load [6–10]. However, a generic sensitivity analysis of such structures with respect to any kind of imperfections requires the introduction of adapted non-deterministic approaches to represent uncertainties. For example, nonlinear stochastic buckling analyses have recently been conducted in which geometrical imperfections [11, 12] were modeled as Gaussian random fields whose statistical properties are issued from available experimental data. Such probabilistic models of uncertainties will be referred to as parametric. More particularly, in the investigation of unstiffened composite cylinders carried out in [12], the knowledge of existing missing composite fibers justified the modeling of material imperfections, which were taken into account with chosen random properties. Despite the accurate modeling of the geometrical imperfections, the buckling load calculated with the nonlinear stochastic computational model was overestimated suggesting that other uncertainties, not considered in the analysis, were present and affected the experimental measurements.

An alternative approach, referred to as the nonparametric probabilistic approach, has been developed for situations in which the uncertainty cannot be singled out in one or a few parameters in the computational model. It allows the consideration of both system-parameter uncertainties and model uncertainties [13]. Note that the nonparametric approach has been extended to uncertain nonlinear reduced-order models of geometrically nonlinear structures [14]. The development of such nonlinear reduced-order models requires first the selection of an appropriate deterministic basis for the representation of the response. This basis can be obtained by one of several techniques such as the Proper Orthogonal Decomposition method (POD method) [15–17]. One can also rely on selected linear elastic modes appropriately enriched, see [18] for a recent review. The parameters of the nonlinear reduced-order model of the mean structure can then be either deduced using the STEP procedure (which is based on the smart non-intrusive use of standard commercial finite element codes) [14, 18, 19] or from explicit construction as shown in [20] in the context of three-dimensional solid finite elements. Having established the reduced-order model of the mean structure, uncertainties on the linear and on the nonlinear parts of the stiffness operator are introduced in the nonparametric framework. This is accomplished through the construction of a dedicated random operator with values in the set of all positive-definite symmetric real matrices whose mean value involves all linear, quadratic and cubic stiffness terms of the mean nonlinear reduced-order model [14]. The resulting stochastic nonlinear computational model is characterized by a single scalar dispersion parameter, quantifying the level of uncertainty in the stiffness properties which can easily be identified with experiments. Experimental validations based on this theory can be found in [20, 21] for slender elastic bodies, e.g. beams and in [22] for cylindrical shells in the context of nonlinear statics.

The paper is organized as follows. Section 2 summarizes the main steps leading to the mean non-linear reduced-order computational model following the approach of [20]. Section 3 is devoted to the construction of the stochastic nonlinear computational model using the nonparametric probabilistic approach for modeling the random uncertainties. A Gaussian non-stationary second-order stochastic process is also introduced to represent the prescribed, earthquake-induced ground-based motions. Finally, the nonlinear post-buckling dynamical analysis of an uncertain cylindrical shell is subjected to the prescribed ground motions is carried out using the methodology presented.

2. REDUCED-ORDER COMPUTATIONAL MODEL USING 3D ELASTICITY IN FINITE DISPLACEMENTS

The structure under consideration is composed of a linear elastic material and is assumed to undergo large deformations inducing geometrical nonlinearities. A total Lagrangian formulation is chosen. Consequently, the dynamical equations are written with respect to the reference configuration. Let Ω be the three-dimensional bounded domain of the physical space $\mathbb{R}^3$ corresponding to the reference configuration taken as a natural state without prestress. The boundary $\partial\Omega$ is such that $\partial\Omega = \Gamma \cup \Sigma$ with $\Gamma \cap \Sigma = \emptyset$ and the external unit normal to boundary $\partial\Omega$ is denoted by $\mathbf{n}$. The boundary part Γ experiences a rigid body displacement induced by a prescribed based motion $\mathbf{u}_\Gamma(\mathbf{x}, t)$ such that $\mathbf{u}_\Gamma(\mathbf{x}, t) = \mathbf{u}_\Gamma(t)\,,\ \forall \mathbf{x} \in \Gamma$. The boundary part Σ is subjected to an external surface force field. Let $\mathbf{x}$ be the position of a point belonging to domain Ω. The relative displacement field expressed with respect to the reference configuration is denoted as $\mathbf{u}(\mathbf{x}, t)$. It should be noted that the surface force field $\mathbf{G}(\mathbf{x}, t)$ acting on boundary Σ and that the body force field $\mathbf{g}(\mathbf{x}, t)$ acting on domain Ω correspond to the Lagrangian transport into the reference configuration of the physical surface force field and to the physical body force field applied on the deformed configuration.

Let $\mathcal{C}$ be the admissible space defined by

$$\mathcal{C} = \{\mathbf{v} \in \Omega\,,\ \mathbf{v} \text{ sufficiently regular }\,,\ \mathbf{v} = \mathbf{0} \text{ on } \boldsymbol{\Gamma}\} \quad . \tag{1}$$

Let $\boldsymbol{\varphi}^\alpha(\mathbf{x})\,,\ \alpha = \{1, \ldots, N\}$, be a finite family of an orthonormal vector basis of $\mathcal{C}$, for which

$$\int_\Omega \varphi_i^\alpha\, \varphi_i^\beta\, d\mathbf{x} = \delta_{\alpha\beta} \quad . \tag{2}$$

The vector $\mathbf{q} = (q_1, \ldots, q_N)$ of the generalized coordinates is introduced as a new set of unknown variables by projecting the nonlinear response $\mathbf{u}(\mathbf{x}, \cdot)$ on the vector space spanned by $\{\boldsymbol{\varphi}^1, \cdots, \boldsymbol{\varphi}^N\}$. Thus, the approximation $\mathbf{u}^N(\mathbf{x}, t)$ of order N of $\mathbf{u}(\mathbf{x}, t)$ is then written as

$$\mathbf{u}^N(\mathbf{x}, t) = \sum_{\beta=1}^{N} \boldsymbol{\varphi}^\beta(\mathbf{x})\, q_\beta(t) \quad , \tag{3}$$

in which $q_\alpha\,,\ \alpha = (1, \ldots, N)$ are solution of the set of nonlinear differential equations

$$\mathcal{M}_{\alpha\beta}\, \ddot{q}_\beta + \mathcal{D}_{\alpha\beta}\, \dot{q}_\beta + \mathcal{K}^{(1)}_{\alpha\beta}\, q_\beta + \mathcal{K}^{(2)}_{\alpha\beta\gamma}\, q_\beta\, q_\gamma + \mathcal{K}^{(3)}_{\alpha\beta\gamma\delta}\, q_\beta\, q_\gamma\, q_\delta = \mathcal{F}^{\text{stat}}_\alpha + \mathcal{F}^{\text{dyn}}_\alpha \quad , \tag{4}$$

with initial conditions

$$\mathbf{q}(0) = \mathbf{0} \quad , \quad \dot{\mathbf{q}}(0) = \mathbf{0} \quad . \tag{5}$$

In Eq.(4), details concerning the expressions of $\mathcal{K}^{(1)}_{\alpha\beta}$, $\mathcal{K}^{(2)}_{\alpha\beta\gamma}$, $\mathcal{K}^{(3)}_{\alpha\beta\gamma\delta}$ and $\mathcal{F}^{\text{stat}}_\alpha$ can be found in [14, 20]. We then have

$$\mathcal{F}^{\text{dyna}}_\alpha = -\int_\Omega \rho\, (\ddot{\mathbf{u}}_\Gamma)_i\, \varphi_i^\alpha\, d\mathbf{x} \quad , \tag{6}$$

$$\mathcal{M}_{\alpha\beta} = \int_\Omega \rho\, \varphi_i^\alpha\, \varphi_i^\beta\, d\mathbf{x} \quad . \tag{7}$$

The model of the reduced damping operator $\mathcal{D}_{\alpha\beta}$ is chosen here as

$$\mathcal{D}_{\alpha\beta} = \zeta\, \mathcal{K}^{(1)}_{\alpha\beta} \quad , \tag{8}$$

in which ζ is a positive constant. It should be noted that the damping modeling can be changed without difficulties.

The mean (or nominal) nonlinear reduced-order computational model is explicitly defined once the projection basis is chosen. The construction is carried out in the context of the

three-dimensional finite element method. The finite elements are isoparametric solid finite elements with 8 nodes and the numerical integration is carried out with 8 Gauss integration points. The main steps of the procedure, which uses the symmetry properties of the reduced operators, can be found in [20] and are summarized below:

- computation of the elementary contributions of each type of internal forces projected on the vector basis
- finite element assembly of these elementary contributions
- computation of the operators $\mathcal{M}_{\alpha\beta}$, $\mathcal{D}_{\alpha\beta}$, $\mathcal{K}^{(1)}_{\alpha\beta}$, $\widehat{\mathcal{K}}^{(2)}_{\alpha\beta\gamma}$ and $\mathcal{K}^{(3)}_{\alpha\beta\gamma\delta}$ of the mean nonlinear reduced-order model

3. UNCERTAIN COMPUTATIONAL MODEL WITH STOCHASTIC EXCITATION

In this Section, the nonparametric probabilistic approach of uncertainties is used for modeling the uncertainties in the nonlinear computational model and the earthquake excitation is modeled by a nonstationary stochastic process.

3.1 Nonparametric stochastic modeling of uncertainties

The main idea of the nonparametric probabilistic approach is to replace each of the matrices of a given mean reduced computational model by a random matrix whose probability model is constructed from the maximum entropy principle using the available information [13, 23]. In the present geometrical nonlinear context, the nonlinear equations involve nonlinear stiffness operators. Let $P = N(N+1)$. A $(P \times P)$ real symmetric positive-definite matrix $[\mathcal{K}]$, whose entries are expressed as a function of operators $\mathcal{K}^{(1)}_{\alpha\beta}$, $\widehat{\mathcal{K}}^{(2)}_{\alpha\beta\gamma}$ and $\mathcal{K}^{(3)}_{\alpha\beta\gamma\delta}$ is introduced (see [14] for the details) and then allows the nonparametric probabilistic approach, initially introduced in the linear context for positive-definite symmetric operators, to be extended to the geometrically nonlinear context. The mean reduced matrices $[\mathcal{M}]$, $[\mathcal{D}]$, $[\mathcal{K}]$ are then replaced by the random matrices $[\boldsymbol{\mathcal{M}}]$, $[\boldsymbol{\mathcal{D}}]$, $[\boldsymbol{\mathcal{K}}]$ defined on the probability space $(\Theta, \mathcal{T}, \mathcal{P})$ such that $\mathcal{E}\{[\boldsymbol{\mathcal{M}}]\} = [\mathcal{M}]$, $\mathcal{E}\{[\boldsymbol{\mathcal{D}}]\} = [\mathcal{D}]$, $\mathcal{E}\{[\boldsymbol{\mathcal{K}}]\} = [\mathcal{K}]$ in which $\mathcal{E}$ is the mathematical expectation. The random matrices $[\boldsymbol{\mathcal{M}}]$, $[\boldsymbol{\mathcal{D}}]$, $[\boldsymbol{\mathcal{K}}]$ are then written as $[\boldsymbol{\mathcal{M}}] = [L_M]^T [\mathbf{G}_M(\delta_M)] [L_M]$, $[\boldsymbol{\mathcal{D}}] = [L_D]^T [\mathbf{G}_D(\delta_D)] [L_D]$, $[\boldsymbol{\mathcal{K}}] = [L_K]^T [\mathbf{G}_K(\delta_K)] [L_K]$ in which $[L_M]$, $[L_D]$ and $[L_K]$ are $(N \times N)$, $(N \times N)$ and $(P \times P)$ real upper matrices such that $[\mathcal{M}] = [L_M]^T [L_M]$, $[\mathcal{D}] = [L_D]^T [L_D]$ and $[\mathcal{K}] = [L_K]^T [L_K]$. Further, $[\mathbf{G}_M]$, $[\mathbf{G}_D]$ and $[\mathbf{G}_K]$ are full random matrices with values in the set of the positive-definite symmetric $(N \times N)$, $(N \times N)$ and $(P \times P)$ matrices. The probability distributions and the random generators of random matrices $[\mathbf{G}_M(\delta_M)]$, $[\mathbf{G}_D(\delta_D)]$ and $[\mathbf{G}_K(\delta_K)]$ are constructed in [13]. The level of uncertainty is quantified by the dispersion parameter $\boldsymbol{\delta} = (\delta_M, \delta_D, \delta_K)$ defined on a subset Δ of $\mathbb{R}^3$.

3.2 Stochastic excitation

From here on, it is assumed that the ground-based motion is along a given direction. Consequently, the acceleration field in Eq.(6) can be written as $\ddot{\mathbf{u}}_\Gamma(\mathbf{x}, t) = \mathbf{w}_0\, \gamma(t)$, in which $\mathbf{w}_0$ is the unit vector of $\mathbb{R}^3$ characterizing the direction of the ground-based motion, and where $\{\gamma(t), t \geq 0\}$ is a real-valued scalar function. We then can write $\boldsymbol{\mathcal{F}}^{\text{dyna}}(t) = -[L_M]^T [L_T]\, \gamma(t)$, in which $[L_T]$ is the $\mathbb{R}^N$-vector solution of

$$\{[L_M]^T [L_T]\}_\alpha = \int_\Omega \rho\, (\mathbf{w}_0)_i\, \varphi^\alpha_i\, d\mathbf{x} \quad . \tag{9}$$

Note that matrix $[L_M]$ is known and invertible. Consequently, Eq.(9) uniquely defines the vector $[L_T]$. In the earthquake engineering context, the acceleration $\boldsymbol{\gamma}(t)$ induced by the ground-based motion is replaced by the random quantity $\boldsymbol{\Gamma}(t)$ with values in $\mathbb{R}$. Note that $\boldsymbol{\mathcal{F}}^{dyna}(t)$ depends on the structural mass distribution of the structure. Given the fact that there exists uncertainty on this distribution, the vector $[L_M]\,[L_T]$ should not be considered as a deterministic quantity. Consistently with the modeling of the mass matrix, the dynamical load $\boldsymbol{\mathcal{F}}^{\text{dyna}}(t)$ is modeled by the random vector

$$\boldsymbol{\mathcal{F}}^{\text{dyna}}(t) \;=\; -[L_M]^T\,[\mathbf{G}_M(\delta_M)]\,[L_T]\,\boldsymbol{\Gamma}(t) \quad , \tag{10}$$

with values in $\mathbb{R}^N$. The acceleration $\{\boldsymbol{\Gamma}(t), t \geq 0\}$ is modeled here by a Gaussian, non-stationary, centered, second-order stochastic process defined on a probability space $(\Theta', \mathcal{T}', \mathcal{P}')$ which is different from probability space $(\Theta, \mathcal{T}, \mathcal{P})$. Consequently, the stochastic process $\boldsymbol{\Gamma}$ is completely defined by its autocorrelation function $R_{\boldsymbol{\Gamma}}(t,t') \;=\; \mathcal{E}\{\boldsymbol{\Gamma}(t)\,\boldsymbol{\Gamma}(t')\}$. The following usual representation [24] of $\boldsymbol{\Gamma}$ for earthquake accelerogramms is adopted

$$\boldsymbol{\Gamma}(t) \;=\; g(t)\,\boldsymbol{\beta}(t) \quad , \tag{11}$$

in which the function $g(t)$ is the envelope function whose representation can be found in [24–26]. Further, $\{\boldsymbol{\beta}(t), t \in \mathbb{R}\}$ is a real-valued Gaussian, stationary, centered, second-order stochastic process for which the power spectral density function $S_{\boldsymbol{\beta}}(\omega)$ can be written as a rational function [27]. We then have

$$R_{\boldsymbol{\Gamma}}(t,t') \;=\; g(t)\,g(t')\,R_{\boldsymbol{\beta}}(t-t') \quad , \tag{12}$$

where $R_{\boldsymbol{\beta}}(t-t')$ is the autocorrelation function of stochastic process $\boldsymbol{\beta}(t)$ such that

$$R_{\boldsymbol{\beta}}(t-t') \;=\; \int_{\mathbb{R}} S_{\boldsymbol{\beta}}(\omega)\,e^{i\omega(t-t')}\,d\omega \quad . \tag{13}$$

Let $\mathbb{\Gamma}$ be the $(n_t \times 1)$ vector defined by $\mathbb{\Gamma} \;=\; (\Gamma(t_1), \ldots \Gamma(t_{n_t}))$. We introduce the time sampling $t_i \;=\; (i-1)\Delta t\,,\; i \;=\; \{1, \ldots, n_t\}$, of $[0,T]$ with $T \;=\; n_t\,\Delta t$. Then denote by $[R_{\mathbb{\Gamma}}] \;=\; \mathcal{E}\{\mathbb{\Gamma}\,\mathbb{\Gamma}^T\}$ the correlation matrix of $\mathbb{\Gamma}$, which can be evaluated from $R_{\boldsymbol{\beta}}(t)$ of Eq.(13), by Fast Fourier Transform (FFT). The random vector $\mathbb{\Gamma}$ can accordingly be written as

$$\mathbb{\Gamma} \;=\; [L]\,\mathbf{Z} \quad , \tag{14}$$

in which $[L]$ is such that $[R_{\mathbb{\Gamma}}] \;=\; [L]^T\,[L]$. Further, $\mathbf{Z} \;=\; (\mathbf{Z}_1, \ldots \mathbf{Z}_{n_t})$ is a Gaussian random vector such that $\mathcal{E}\{\mathbf{Z}_j\} \;=\; 0$, $\mathcal{E}\{\mathbf{Z}_j^2\} \;=\; 1$ and $\mathbf{Z}_1, \ldots, \mathbf{Z}_{n_t}$ are statistically independent. Note that Eq.(14) allows a generator of independent realizations $\mathbf{Z}(\theta')$ of $\mathbf{Z}$ to be constructed.

3.3 Stochastic nonlinear computational model with random uncertainties

Let $\{\mathbf{U}(\mathbf{x},t)\,, x \in \Omega\,,\; t \geq 0\}$ be the $\mathbb{R}^n$-valued, non-stationary in time, second-order stochastic process, defined on the product of probability spaces $(\Theta, \mathcal{T}, \mathcal{P})$ and $(\Theta', \mathcal{T}', \mathcal{P}')$. For $t \geq 0$, for all θ in Θ and for all θ' in Θ', a realization of the stochastic response is represented by its approximation $\mathbf{U}^N(\mathbf{x}, t; \theta, \theta')$ of order N such that

$$\mathbf{U}^N(\mathbf{x}, t; \theta, \theta') \;=\; \sum_{\beta=1}^{N} \boldsymbol{\varphi}^{\beta}(\mathbf{x})\,\mathbf{Q}_{\beta}(t; \theta, \theta') \quad , \tag{15}$$

in which $\mathbf{Q}(t; \theta, \theta') \;=\; (\mathbf{Q}_1(t; \theta, \theta'), \cdots, \mathbf{Q}_N(t; \theta, \theta'))$ is the solution of the following nonlinear differential equation

$$\begin{aligned}
\mathcal{M}_{\alpha\beta}(\theta)\,\ddot{\mathbf{Q}}_\beta(t;\theta,\theta') \;+\; \mathcal{D}_{\alpha\beta}(\theta)\,\dot{\mathbf{Q}}_\beta(t;\theta,\theta') \quad + \\
\mathcal{K}^{(1)}_{\alpha\beta}(\theta)\,\mathbf{Q}_\beta(t;\theta,\theta') + \mathcal{K}^{(2)}_{\alpha\beta\gamma}(\theta)\mathbf{Q}_\beta(t;\theta,\theta')\,\mathbf{Q}_\gamma(t;\theta,\theta') \quad + \\
\mathcal{K}^{(3)}_{\alpha\beta\gamma\delta}(\theta)\mathbf{Q}_\beta(t;\theta,\theta')\,\mathbf{Q}_\gamma(t;\theta,\theta')\,\mathbf{Q}_\delta(t;\theta,\theta') \;=\; \mathcal{F}_\alpha(t;\theta,\theta')\,,
\end{aligned} \tag{16}$$

with initial conditions

$$\mathbf{Q}(0;\theta,\theta') \;=\; \mathbf{0} \quad , \quad \dot{\mathbf{Q}}(0;\theta,\theta') \;=\; \mathbf{0} \quad . \tag{17}$$

In Eq.(16), the quadratic stiffness term is written as

$$\mathcal{K}^{(2)}_{\alpha\beta\gamma}(\theta) \;=\; \frac{1}{2}(\widehat{\mathcal{K}}^{(2)}_{\alpha\beta\gamma}(\theta) + \widehat{\mathcal{K}}^{(2)}_{\beta\gamma\alpha}(\theta) + \widehat{\mathcal{K}}^{(2)}_{\gamma\alpha\beta}(\theta)) \quad . \tag{18}$$

Note that the random linear, quadratic and cubic stiffness terms $\mathcal{K}^{(1)}_{\alpha\beta}$, $\widehat{\mathcal{K}}^{(2)}_{\alpha\beta\gamma}$ and $\mathcal{K}^{(3)}_{\alpha\beta\gamma\delta}$ are easily deduced from the random matrix $[\mathcal{K}]$ using the reshaped operations described in [14]. With regard to the numerical solver used for computing the nonlinear coupled differential equation, a Newmark method is used [28], which employs the averaging acceleration scheme known to be unconditionally stable. With this solver, a set of nonlinear algebraic equations must be solved at each sampling time. This computation is addressed by the fixed-point method or by the Crisfield arc-length method [29] (the fixed-point is favored but if not convergent, it is replaced by the Crisfield algorithm).

4. NUMERICAL APPLICATION

The methodology is applied on a thin cylindrical shell, which is modeled here using three-dimensional solid finite elements. In the present context, despite the very small thickness of the investigated structure, the choice of 3D solid finite elements is preferred to the more natural choice of shell finite elements for the following reasons:

- It is more exact to use a 3D nonlinear elasticity theory than a thin shell nonlinear elasticity theory.
- In the context of the construction of a reduced-order model, it is easier to compute the terms constituting Eq.(4).
- Finally, the computational cost increase, associated with the larger number of DOFs, is not a real obstacle, given the current computational capabilities and the possibility of using parallel computations.

4.1 Finite element model

The three-dimensional structure is modeled by a circular cylindrical shell of height $h = 0.144\,m$, mean radius $0.125\,m$ and thickness $2.7\times10^{-4}\,m$. Its bottom experiences a rigid body displacement and the upper ring is rigid with three DOFs in translation. The isotropic linear elastic material properties and the mass density have been experimentally measured [9, 30] to be $E = 1.8\times10^{11}\,N.m^{-2}$, $\nu = 0.3$ and $\rho = 8\,200\,Kg\times m^{-3}$. The structure is subjected to a constant traction point load $F^{\,\mathrm{stat}}$ applied along $\mathbf{e}_3$ at $x_3 = h$. Since a concentrated mass $M' = 80\,Kg$ is added at the free node located at the top of the shell along direction $\mathbf{e}_2$, the dynamical load $F^{\,\mathrm{dyna}}(t)$ has its main contribution at the top of the shell along direction $\mathbf{e}_2$. This allows to reproduce the experimental conditions as described in [9, 30]. From that, it can be deduced that the use of the static POD basis, which strongly depends on the choice of

the static shear load, for the present dynamic case is appropriate because the dynamic shear load induced by the ground motion and the static shear load used in [9] belong to the same loading class.

The finite element model is a regular mesh composed of $(n_r - 1) \times n_\theta \times (n_3 - 1) = 1 \times 7\,500 \times 9599 = 712\,500$ 8-nodes solid finite elements with 8 Gauss integration points. The mean computational model thus has 4 230 003 degrees of freedom. should be noted that, for the given class corresponding to the use of 8 nodes solid finite elements, a sensitivity analysis has been made in [22] in the static nonlinear context with respect to thickness e, to the choice of boundary conditions, and to parameters n_θ and n_3 controlling the precision of the mesh. The present choice of the parameters corresponds to the closest situation with respect to the experimental data available in [8].

The observation is the displacement of the node *obs*, corresponding to the location of the experimental observation along $\mathbf{e}_2$ (the direction of the shear point load) and is denoted by $u_{obs}(s)$.

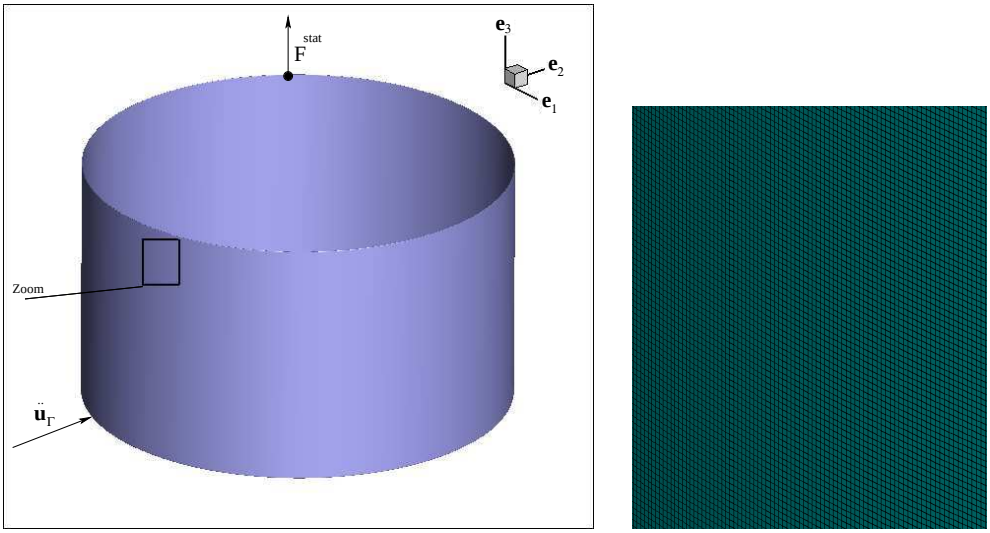

Figure 1: Left part: 3D representation of the cylindrical shell with boundary conditions ($\circ$ denotes the only free node of the upper bound of the cylindrical shell, corresponding to the node *obs*). Right part : zoom of the mesh.

A geometrical perturbation taken as the linear buckling mode shape calculated for a critical shear load located at the top of the shell along direction $\mathbf{e}_2$ is added to the structure with a maximum amplitude of $2.7\times10^{-4}\ m$ [9]. It thus allows the buckling to be numerically induced.

The random operators of the stochastic nonlinear computational model, defined on probability space $(\Theta, \mathcal{T}, \mathcal{P})$ are constructed as explained in the previous Section. Uncertainties on the mass distribution is negligible and uncertainties concerning damping are small. The results concerning a previous static experimental identification of the nonlinear stochastic computational model are used [22], so that the stiffness uncertainty level is fixed to $\delta_K = \delta_K^{opt} = 0.45$. The dynamic loading conditions consist in a seismic horizontal motion applied to the base of the cylindrical shell. Since the mass is assumed to be certain, the corresponding shear load is a stochastic process indexed by $\mathbb{R}^+$ and defined on probability space $(\Theta', \mathcal{T}', \mathcal{P}')$. Consequently, the stochastic physical response is modeled by $\mathbb{R}^n$-random nonlinear stochastic process $\{\mathbf{U}(t), t \in \mathbb{R}^+\}$ defined on the product of probability spaces $(\Theta, \mathcal{T}, \mathcal{P})$ and $(\Theta', \mathcal{T}', \mathcal{P}')$.

4.2 Definition of the stochastic excitation and of the frequency band of analysis

The stochastic excitation is simulated as explained in Section 3.1. For the present application, the power spectral density $S_\beta(\omega)$ of the stochastic process $\beta(t)$ is chosen as

$$S_\beta(\omega) = \overline{s}\frac{\overline{\omega}^4 + 4\overline{\xi}^2\overline{\omega}^2\omega^2}{(\omega^2 - \overline{\omega}^2)^2 + 4\overline{\xi}^2\overline{\omega}^2\omega^2} \quad , \tag{19}$$

in which $\overline{s} = 1.15 \times 10^{-4}\, m^2.s^{-3}$, $\overline{\omega} = 785.4\, rad.s^{-1}$ and $\overline{\xi} = 0.02$. The frequency band of analysis is $\mathbb{B}_\nu = [0\,,\,160]\, Hz$. The time sampling is $\delta t = 5 \times 10^{-4}\, s$, the total time duration $T = 1.27\, s$ and therefore, the number of time steps is $n_t = 2546$. The frequency resolution is $\delta\nu = 0.78\, Hz$ corresponding to a frequency band $[0\,,\,1000]\, Hz$ (the sampling frequency is $\nu_e = 2000\, Hz$). The envelope function is a piecewise continuous function defined by $g(t) = 25\, t^2/4$ if $t < 0.4\, s$, $g(t) = 1$ if $t \in [0.4\,,\,0.7]\, s$ and $g(t) = e^{-10(t-0.7)}$ if $t > 0.7\, s$. Figure 2 displays a typical realization $\mathbf{\Gamma}(\theta', t)$ of the stochastic process $\mathbf{\Gamma}(t)$. The stochastic excitation is then obtained using Eq.(10).

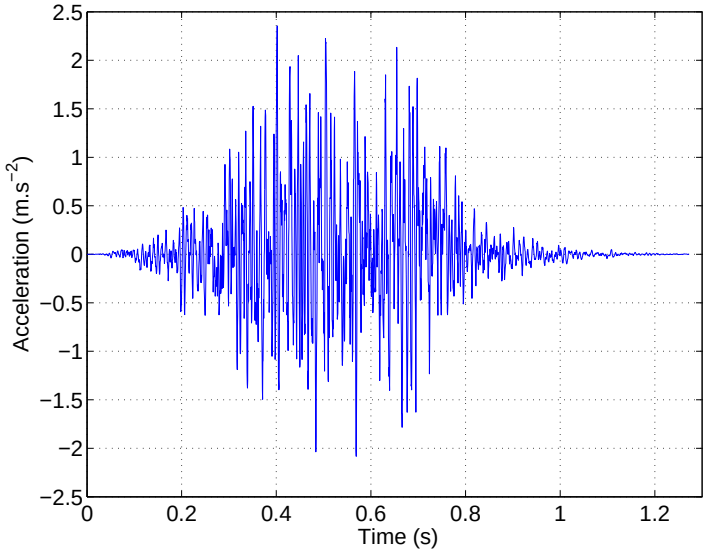

Figure 2. Realization of stochastic process $\mathbf{\Gamma}(t)$

4.3 Construction of the mean nonlinear reduced-order computational model

For the considered nonlinear elasto-dynamic problem, there are two notable strategies for constructing the projection basis of the mean nonlinear reduced-order computational model. A first one uses the POD method and thus requires full computations of the elasto-dynamical reference response with the nonlinear computational model. A second strategy consists in solving the usual generalized eigenvalue problem of the linearized computational model and selecting a set of its linear eigenmodes of vibration as projection basis. Once this basis is built according to either of the above strategies, the mean nonlinear reduced operators are constructed by the methodology of Section 2.

In [20], the POD projection basis obtained from the nonlinear static reference calculation of a structure was used as the projection basis for constructing the mean nonlinear reduced-order computational model of the structure. Such method has also been used in [22] for the nonlinear static analysis of the present cylindrical shell. It would be interesting to reuse such POD projection basis obtained in the context of a nonlinear static case for the present nonlinear dynamic case. Since the convergence rate of the solution constructed with such

a projection basis strongly depends on the external applied loads, it is appropriate only if a similar loading class is used. With the presence of the concentrated mass M' at the top of the structure, the shear load induced by the ground-based motion is largest at the top of the structure. This excitation, in addition to the external constant traction load, is compatible with the loading used for the nonlinear static case in [22]. Specifically, let $\mathcal{R}^{(N)} = \{\boldsymbol{\varphi}^1, \ldots, \boldsymbol{\varphi}^N\}$ be the family composed of the N basis vectors $\boldsymbol{\varphi}^1, \ldots, \boldsymbol{\varphi}^N$ related to the first larger eigenvalues of such static POD basis. In [22], the convergence analysis yields $N = 27$. Note that the family $\mathcal{R}^{(27)}$ is not expected to be sufficient to describe the nonlinear dynamical response of the shell; it needs to be completed by additional basis vectors that we select as linear elastic modes. A usual modal analysis of the linearized dynamical computational model with the predeformation discussed in Section 4.1 is then performed of which some results are summarized in Table 1.

	frequency (Hz)	modal shape
Mode 1	121.10	global
Mode 2	124.16	global
Mode 3	897.02	local
Mode 4	897.06	local

Table 1. Eigenfrequencies and type of elastic modes

Owing to the slight predeformation of the structure, according to the first linear buckling mode, the structure is not perfectly axisymmetric and pairs of distinct eigenfrequencies are obtained as seen in Table 1. An analysis of the first 40 eigenfrequencies and mode reveals that the first two modes $\widetilde{\boldsymbol{\varphi}}^1$ and $\widetilde{\boldsymbol{\varphi}}^2$ describe global bending modes of the structure as shown in Fig. 3, see Table 1.

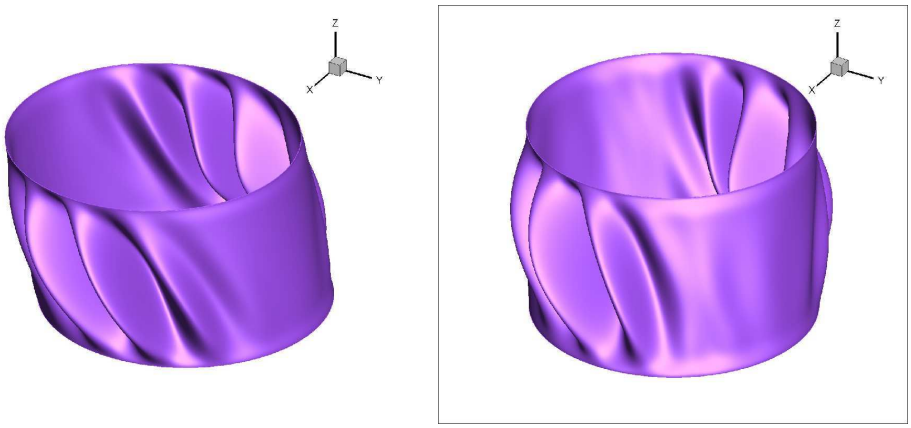

Figure 3. Elastic mode related to eigenfrequencies $f_1 = 121.10\,Hz$ and $f_2 = 124.16\,Hz$

Further, a high modal density is observed, starting with eigenfrequency $\nu_3 = 897.01\,Hz$. There are 38 local elastic modes belonging to frequency band $[897\,,\,1123]\,Hz$. The ground motions characterized by the power spectral density of Eq.(19) would strongly excite the first two elastic modes but only weakly the ensuing ones. Thus the projection basis of the stochastic nonlinear reduced-order model must closely represent the first two elastic modes but not necessarily the ensuing ones. To assess this issue, the representation of elastic mode $\widetilde{\boldsymbol{\varphi}}^\beta$, $\beta \in \{1, 2\}$ on $\mathcal{R}^{(27)}$ has been determined. It can be shown that elastic mode $\widetilde{\boldsymbol{\varphi}}^1$ is poorly represented on $\mathcal{R}^{(27)}$ and that although the error related to elastic mode $\widetilde{\boldsymbol{\varphi}}^2$ is smaller, due to the coexistence of local and global contributions, it was deemed too large to be neglected. As a consequence, these two elastic modes were selected in order to enrich $\mathcal{R}^{(27)}$. The final

projection basis is the family $\mathcal{S}^{(29)} = \mathcal{R}^{(27)} \bigcup \{\boldsymbol{\varphi}^{28}, \boldsymbol{\varphi}^{29}\}$, in which the vectors $\boldsymbol{\varphi}^{\alpha}$, for $\alpha \in \{28, 29\}$ are defined as

$$\boldsymbol{\varphi}^{\alpha} = \frac{\boldsymbol{\psi}^{\alpha}}{\|\boldsymbol{\psi}^{\alpha}\|} \quad , \quad \boldsymbol{\psi}^{\alpha} = \widetilde{\boldsymbol{\varphi}}^{\alpha-27} - \sum_{i=1}^{\alpha-1} \frac{(\boldsymbol{\varphi}^{i})^{T}\, \widetilde{\boldsymbol{\varphi}}^{\alpha-27}}{\|\boldsymbol{\varphi}^{i}\|^{2}} \boldsymbol{\varphi}^{i} \quad , \tag{20}$$

according to a partial Gram-Schmidt orthonormalization procedure. Note that this projection basis verifies Eq. (2). The mean reduced-order computational model is then obtained using the enriched projection basis composed by the family $\mathcal{S}^{(29)}$. It should be noted that the first eigenfrequency is computed with the linearized computational model projected on $\mathcal{S}^{(29)}$, are $\nu'_1 = 121.19\,Hz < \nu'_2 = 124.57\,Hz < \nu'_3 = 1602.96\,Hz < \nu'_4 = 1768.25\,Hz$. As expected, ν'_1 and ν'_2 are close to their original counterparts ν_1 and ν_2, see Table 1. The reduced dissipation matrix is constructed according to Eq.(8) by choosing $\zeta = 4.44 \times 10^{-5}$. This leads to a critical dissipation rate $\xi \simeq 0.017$ for the two first elastic modes.

4.4 Results

The response of the shell is monitored as the same position and in the same direction than above, see Section 4.2. This random observation, denoted by $U_{obs}(t)$, is a stochastic process indexed by $[0, T]$ and defined on the product of probability spaces $(\Theta, \mathcal{T}, \mathcal{P})$ and $(\Theta', \mathcal{T}', \mathcal{P}')$. It can then be written as

$$U_{obs}(t) = \underline{u}_{obs}(t) + U^{c}_{obs}(t) \quad , \tag{21}$$

in which $\underline{u}_{obs}(t)$ is the deterministic function characterizing the mean of the stochastic nonlinear dynamical response i.e.

$$\underline{u}_{obs}(t) = \mathcal{E}\{U_{obs}(t)\} = \int_{\Theta} \int_{\Theta'} U_{obs}(t, \theta, \theta')\, d\mathcal{P}(\theta)\, d\mathcal{P}'(\theta') \quad , \tag{22}$$

and where $U^{c}_{obs}(t)$ is a centered non-stationary stochastic process. In the sequel, $U_{obs}(t, \theta, \theta')$ is denoted by $U_{obs}(t; \Theta)$, where $\Theta = (\theta, \theta')$.

Four analysis cases (see Table 2) are investigated, analyzed and compared.

	Stiffness	Stiffness	External load
Case 1	linear	deterministic	stochastic
Case 2	linear	stochastic	stochastic
Case 3	nonlinear	deterministic	stochastic
Case 4	nonlinear	stochastic	stochastic

Table 2. Description of the analysis cases

Figure 4 displays the graphs of $t \mapsto U^{c}_{obs}(t, \Theta)$ (gray line) and $t \mapsto \underline{u}_{obs}(t)$ (black line) for the four analysis cases and for a specific realization of the ground motions related to Fig. 2. It is seen that $\underline{u}_{obs}(t)$ is a centered oscillating function for the linear cases as expected given the zero mean character of the excitation. However, a small negative mean is observed for the nonlinear cases. Superimposing all cases, it is seen, for this present realization, that the geometric nonlinear effects occur first at $t_{nonlin} = 0.16\,s$ for a displacement level greater than $1.8 \times 10^{-4}\,m$, or $\frac{2}{3}$ of the shell thickness. Comparing cases 1 and 2 with cases 3 and 4 respectively, it is seen that the effect of the geometrical nonlinearities is to decrease the intensity of the response. Moreover, this effect increases with the presence of model and system-parameter uncertainties in the stochastic computational model. Comparing case 1 with case 2, it is seen that the presence of random uncertainties significantly spreads the

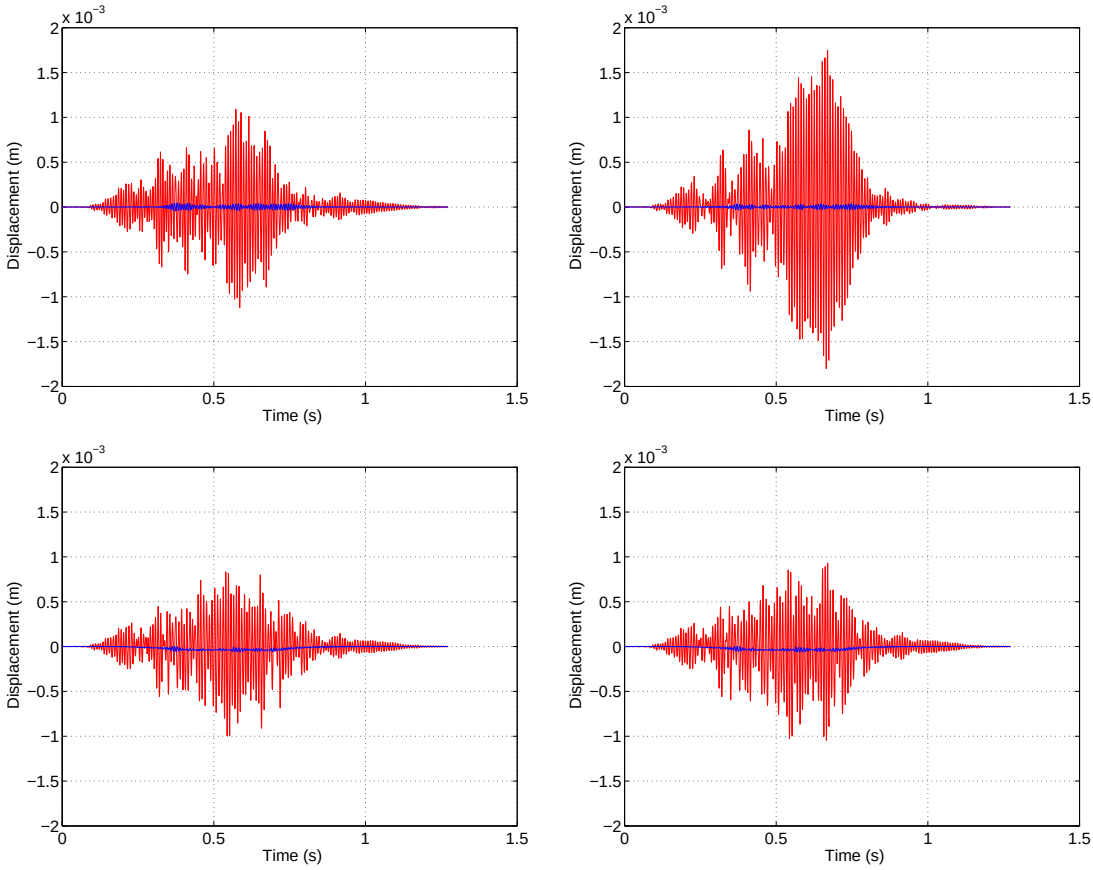

Figure 4: Graphs of functions $t \mapsto U^c_{obs}(t, \mathbb{0})$ (gray line) and $t \mapsto \underline{u}_{obs}(t)$ (black line) for cases 1 and 2 (upper graphs) and for cases 3 and 4 (lower graphs)

stochastic linear response allowing displacements of $1.7 \times 10^{-3}\, m$, or 6 thicknesses, to occur. A similar conclusion does not seem to hold in the nonlinear case : when comparing case 3 with case 4, the presence of random uncertainties only seems to slightly modify the nonlinear dynamical response.

The complex instantaneous spectral density function $s_{U^c_{obs}}(\nu, t)$ of the nonstationary stochastic process $\{U^c_{obs}(t)\,,\, t \in [0\,,\, T\,]\}$ is defined as

$$s_{U^c_{obs}}(\nu, t) \;=\; \frac{1}{2\pi} \int_0^T e^{-2\,i\pi\nu t'}\, r_{U^c_{obs}}(t', t)\, dt' \quad , \tag{23}$$

in which $r_{U^c_{obs}}(t, t') \;=\; \mathcal{E}\{U^c_{obs}(t)\, U^c_{obs}(t')\}$ is the autocorrelation function of stochastic process $U^c_{obs}(t)$. It should be noted that the numerical estimation of $s_{U^c_{obs}}(\nu, t)$ can be carried out by using the periodogram method with a Tukey-Hanning time window combined to FFT [31, 32]. Then,

$$s_{U_{obs}}(\nu, t) \;=\; \frac{1}{2\pi} \hat{\underline{u}}_{obs}(\nu)\, \underline{u}_{obs}(t) + s_{U^c_{obs}}(\nu, t) \quad , \tag{24}$$

with $\hat{\underline{u}}_{obs}(\nu) \;=\; \displaystyle\int_0^T e^{-2\,i\pi\nu\, t'}\, \underline{u}_{obs}(t')\, dt'$.

The analysis is next focused on the fixed time $t_0 \;=\; 0.5\, T$ and in the frequency band $[80\,,\, 160]\, Hz$ around the resonances. Figure 5 shows the graph $\nu \mapsto log_{10}(|s_{U_{obs}}(\nu, t_0)|)$ for the linear case (left graph) and for the nonlinear case (right graph). The presence of random uncertainties spreads the resonance in the linear case whereas no such effect is noticed in the nonlinear case. Comparing the peak frequencies of cases 1 and 3, a shift of the resonance from $120\, Hz$ until $113\, Hz$ is observed, which shows that the presence of geometrical

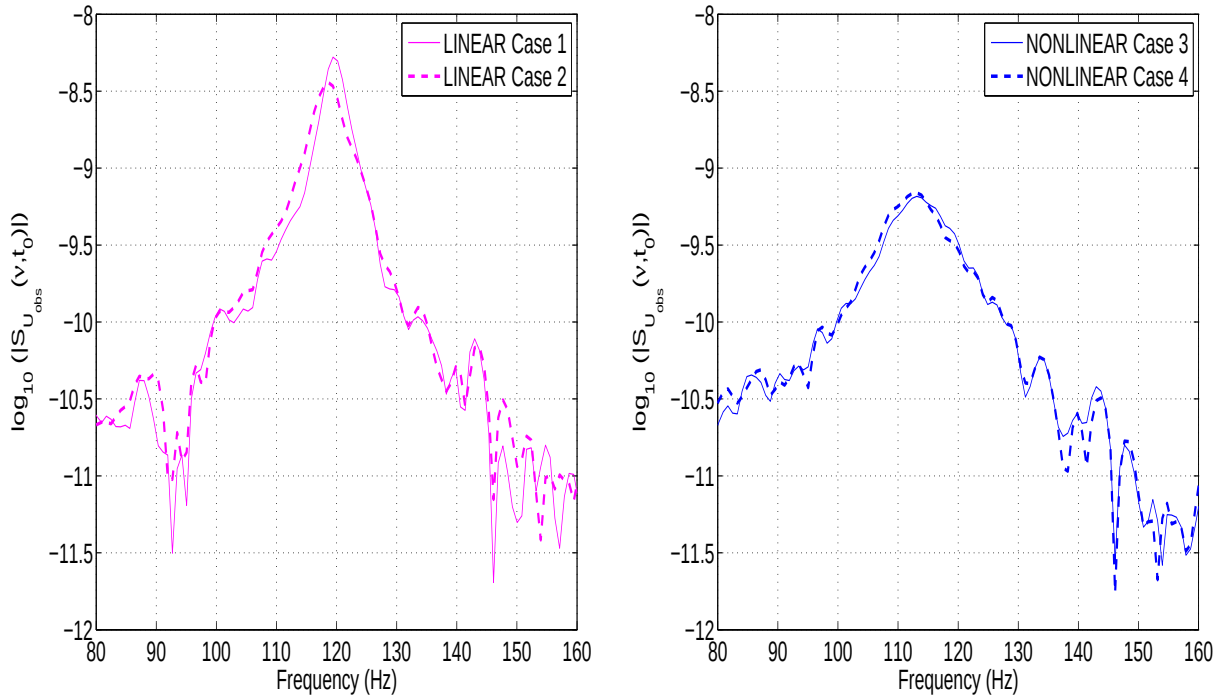

Figure 5: Graphs of $\nu \mapsto \log_{10}(|s_{U_{obs}}(\nu, t_0)|)$ without and with random uncertainties (thin line and thick dashed line): linear case (left graph) and nonlinear case (right graph).

nonlinearities induces a softening effect. Moreover, the presence of geometrical nonlinearities yields a peak broadening and a decrease of the resonance magnitude from $-8.3\,dB$ until $-9.16\,dB$. Comparing case 2 (or 4) with case 1 (or 3), it is seen that the presence of uncertainties have a moderate effect on the response. For the linear case, the presence of uncertainties shifts the peak of response from $120\,Hz$ to $118\,Hz$ and reduces its magnitude by $0.2\,dB$. This small effect can be explained as follows: in case 2, the random linear $(N\times N)$ reduced stiffness operator is extracted from the $(P \times P)$ random reshaped stiffness operator $[\mathcal{K}]$, for which the dispersion parameter δ has been identified to 0.45. Let δ^{LIN} be the effective dispersion parameter related to this random linear $(N\times N)$ reduced stiffness operator. Since $N \ll P = N(N+1)$, it can be shown that $\delta^{LIN} = 0.025$. Consequently, the random response of the linearized system with uncertainties is computed with a small level ($\delta^{LIN} = 0.025$) of uncertainties. This small level of the dispersion parameter is then coherent with the observed slight impact of the random uncertainties on the linear dynamical response. In the nonlinear case, only a change of $0.03\,dB$ can be observed in the peak response magnitude. For both nonlinear and linear cases, the complex instantaneous spectral density function appears weakly sensitive to random uncertainties. This can be explained by the fact that this quantity of interest is issued from a statistical averaging of the random observation over the two statistical sources of the randomness (the excitation and the variability induced by uncertainties).

From here on, for $t \in [0\,,\,T]$, for $\theta \in \Theta$ and for $\theta' \in \Theta'$, a realization of the stochastic process $U_{obs}(t)$ is denoted by $U_{obs}(t;\theta,\theta')$. To better understand and analyze the effects of random uncertainties on the nonlinear stochastic response, a spectral analysis of the nonstationary observation $U_{obs}(t)$ is next. To this end, let

$$S_{U_{obs}}(\nu, t; \theta) = \frac{1}{2\pi} \int_0^T e^{-2i\pi\nu t'} R_{U_{obs}}(t', t; \theta)\, dt' \quad , \tag{25}$$

be a sample of the complex-valued random instantaneous spectral density function for ν in $\mathbb{B}_\nu$, for t in $[0\,,\,T]$ and for θ in Θ. In this equation, for all fixed t and t', $\theta \mapsto R_{U_{obs}}(t, t'; \theta)$ is

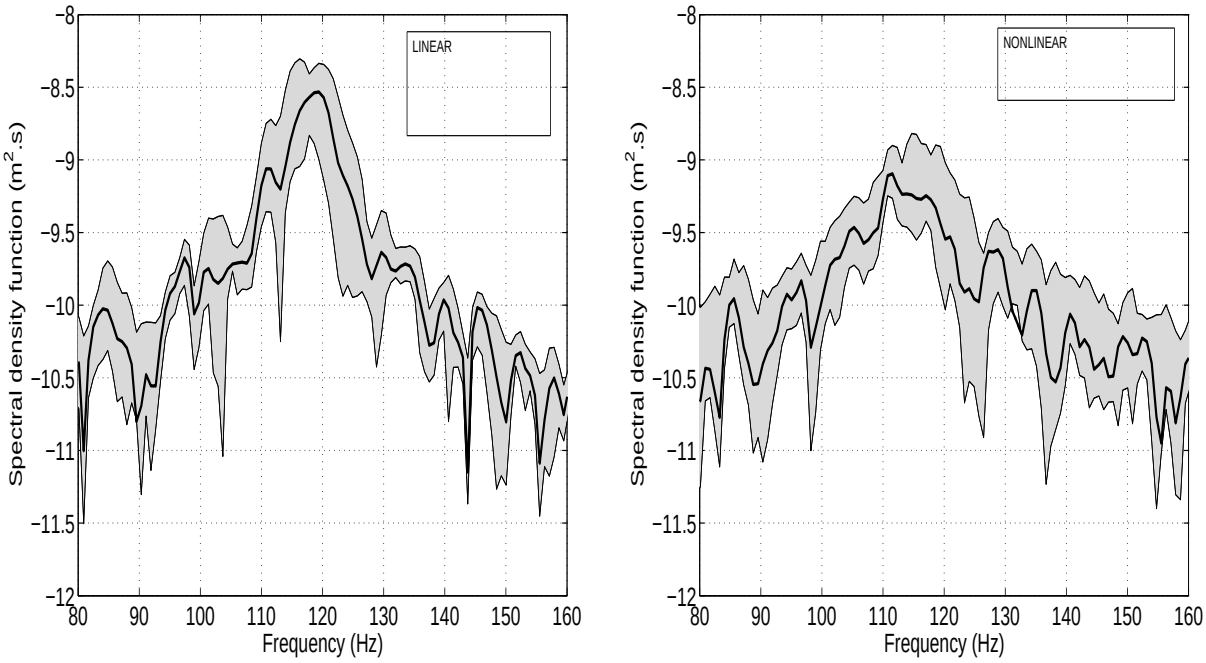

Figure 6: Confidence region: graph of $\nu \mapsto log_{10}(\mathbb{E}\{|S_{U_{obs}}(\nu, t_0)|\})$ (thick line) and graph of the confidence region of $\nu \mapsto log_{10}(|S_{U_{obs}}(\nu, t_0)|)$ (grey region). Linear case (left graph) and nonlinear case (right graph).

the real-valued random variable defined by

$$R_{U_{obs}}(t, t'; \theta) = \int_{\Theta'} U_{obs}(t; \theta, \theta')\, U_{obs}(t'; \theta, \theta')\, d\mathcal{P}'(\theta') \quad . \tag{26}$$

Therefore, $\{S_{U_{obs}}(\nu, t), \nu \in \mathbb{B}_\nu, t \in [0, T]\}$ is a second-order stochastic process defined on probability space $(\Theta, \mathcal{T}, \mathcal{P})$.

Figure 6 shows the graph of the confidence region calculated with a probability level $P_c = 0.95$ of the random stochastic process $\nu \mapsto log_{10}(|S_{U_{obs}}(\nu, t_0)|)$ for the linear case (left graph) and for the nonlinear case (right graph). Note that the computations have been carried out for $77 \times 77 = 5929$ realizations (θ, θ'). It should be noted that the figure only gives a global trend of the results, since the confidence region remain not smooth enough to state that convergence with respect to the number of simulations is reached. It can be seen that the peak response corresponding to the nonlinear case occurs for a lower frequency and with a smaller magnitude than its linear counterpart. Furthermore, the confidence region related to the nonlinear case is broader, demonstrating that the nonlinear case is less robust than the linear one with respect to uncertainties. Note that such result was expected because of the high energy transfer induced by the nonlinearities.

CONCLUSION

The paper has presented an advanced computational method for analyzing the nonlinear dynamic post-buckling behavior of a geometrically nonlinear thin shell structure in presence of uncertainties. The nonlinear stochastic computational model has been used for predicting the nonlinear dynamical post-buckling response, under a stochastic excitation induced by a ground-based motion of the structure. The influence of geometrical nonlinearities has been analyzed through instantaneous spectral density functions. It is concluded that the presence of geometrical nonlinearities modifies the dynamical behavior (1) by inducing a local soften-

ing effect and a decrease of the resonance magnitude; (2) by decreasing the robustness of the response predictions with respect to uncertainties.

REFERENCES

[1] J.W. Hutchinson. Buckling and initial postbuckling behaviour of oval cylindrical shells under axial compression. *ASME Journal of Applied Mechanics*, 35(1):66–76, 1968.

[2] R.C. Tennyson and K.C. Chan. Buckling of imperfect sandwich cylinders under axial compression. *International Journal of Solids and Structures*, 26:1017–1036, 1990.

[3] P. Mandal and R. Calladine. Buckling of thin cylindrical shells under axial compression. *International Journal of Solids and Structures*, 37(33):4509–4525, 2000.

[4] H. Huang and Q. Han. Research on nonlinear postbuckling of functionally graded cylindrical shells under radial loads. *Computers & Structures*, 92(6):1352–1357, 2010.

[5] L. Chen and J.M. Rotter. Buckling of anchores cylindrical shells of uniform thickness under wind load. *Engineering Structures*, 41:199–208, 2012.

[6] S. Matsuura, H. Nakamura, K. Kokubo, S. Ogiso, and H. Ohtsubo. Shear-bending buckling analyses of fast breeder reactor main vessels. *Nuclear Engineering and Design*, 153:305–317, 1995.

[7] J. Okada, K. Iwata, K. Tsukimori, and T. Nagata. An evaluation method for elastic-plastic buckling of cylindrical shells under shear forces. *Nuclear Engineering and Design*, 157:65–79, 1995.

[8] G. Michel, A. Combescure, and J.-F. Jullien. Finite element simulation of dynamic buckling of cylinders subjected to periodic shear. *Thin-Walled Structures*, 36:111–135, 2000.

[9] G. Michel, A. Limam, and J.-F. Jullien. Buckling of cylindrical shells under static and dynamic shear loading. *Engineering Structures*, 22:535–543, 2000.

[10] W Schneider and Y Ribakov. Collapse analysis of thin walled cylindrical steel shell subjected to constant shear stress. *Computers & Structures*, 82(29-30):2463–2470, 2004.

[11] C.A. Schenk and G.I. Schuëller. Buckling analysis of cylindrical shells with random geometric imperfections. *International Journal of Nonlinear Mechanics*, 38(7):1119–1132, 2003.

[12] M. Broggi and G.I. Schuëller. Efficient modeling of imperfections for buckling analysis of composite cylindrical shells. *Engineering Structures*, 33:1796–1806, 2011.

[13] C. Soize. *Stochastic Models of Uncertainties in Computational Mechanics, Lecture Notes in Engineering Mechanics 2*. American Society of Civil Engineers (ASCE), 2012.

[14] M.-P. Mignolet and C. Soize. Stochastic reduced order models for uncertain geometrically nonlinear dynamical systems. *Computer Methods in Applied Mechanics and Engineering*, 197:3951–3963, 2008.

[15] L Sirovich. Turbulence and the dynamics of coherent structures . *Quarterly of Applied Mathematics*, 45(3):561–571, 1987.

[16] R. Sampaio and C. Soize. Remarks on the efficiency of pod for model reduction in nonlinear dynamics of continuous elastic systems. *International Journal for Numerical Methods in Engineering*, 72(1):22–45, 2007.

[17] M.F.A Azeez and A.-F. Vakakis. Proper orthogonal decomposition (POD) of a class of vibroimpact oscillations. *Journal of Sound and Vibration*, 240(5):859–889, 2001.

[18] M.-P. Mignolet, A. Przekop, S.A. Rizzi, and S.M. Spottswood. A review of indirect/non-intrusive reduced order modeling of nonlinear geometric structures. *Journal of Sound and Vibration, accepted for publication, http://dx.doi.org/10.1016/j.jsv.2012.10.017*, 2012.

[19] A.A. Muryavov and S.A. Rizzi. Determination of nonlinear stiffness with application to random vibration of geometrically nonlinear structures. *Computers & Structures*, 81:1513–1523, 2003.

[20] E. Capiez-Lernout, C. Soize, and M.-P. Mignolet. Computational stochastic statics of an uncertain curved structure with geometrical nonlinearity in three-dimensional elasticity. *Computational Mechanics*, 49(1):87–97, 2012.

[21] R. Murthy, X.Q. Wang, R. Perez, M.-P. Mignolet, and L.A. Richter. Uncertainty-based experimental validation of nonlinear reduced order models. *Journal of Sound and Vibration*, 331, 2012.

[22] E. Capiez-Lernout, C. Soize, and M.-P. Mignolet. Uncertainty quantification for post-buckling analysis of cylindrical shells with experimental comparisons. In *European Congress of Computational Methods in Applied Science and Engineering, ECCOMAS 2012, Wien (Austria), 10-15 September 2012*, 2012.

[23] C. Soize. Random matrix theory for modeling random uncertainties in computational mechanics. *Computer Methods in Applied Mechanics and Engineering*, 194(12-16):1333–1366, 2005.

[24] P. Kree and C. Soize. *Mathematics of random phenomena random vibrations of mechanical structures*. D. Reidel Pub. Co., 1986.

[25] G.R. Saragoni and G.C. Hart. Simulation of artificial earthquakes. *Earthquake Engineering and Structural Dynamics*, 2(3):249–267, 1974.

[26] D.M. Boore. Simulation of ground motion using the stochastic method. *Pure and Applied Geophysics*, 160(3-4):635–676, 2003.

[27] H. Kanai. Semi-empirical formula for the seismic characteristics of the ground motion. *Bulletin of the Earthquake Research Institute*, 35:309–325, 1957.

[28] K.J. Bathe. *Finite Element Procedures in Engineering Analysis*. Prentice-Hall, 1982.

[29] M.A. Crisfield. *Non-linear finite element analysis of solids and structures, Vol. 1 : essentials*. John Wiley and Sons, Chichester, 1997.

[30] G. Michel. *Flambage de coques minces cylindriques sous un chargement dynamique de cisaillement*. PhD thesis, INSA Lyon, 1997.

[31] L.C. Ludeman. *Fundamentals of Digital Signal Processing*. Harper and Row, New York, 1986.

[32] C. Soize. *Méthodes mathématiques en analyse du signal*. Masson, 1993.